Electronic Supplementary Material (ESI) for Physical Chemistry Chemical Physics.

Supporting information

First-principles study of line-defect-embedded zigzag graphene nanoribbons: Electronic and magnetic properties

Zhaoyong Guan,[a] *Chen Si,*[b] *Shuanglin Hu,*[c] *Wenhui Duan*[a, d]

[a] Department of Physics, Tsinghua University, Beijing 100084, P. R. China

[b] School of Materials Science and Engineering, Beihang University, Beijing 100191, P. R. China

[c] Institute of Nuclear Physics and Chemistry, China Academy of Engineering Physics, Mianyang, Sichuan 621900, P. R. China

[d] Collaborative Innovation Center of Quantum Matter, Tsinghua University, Beijing 100084, P. R. China

1. The electronic band structures and magnetic configuration of H-14-2H ZGNR for the AFM-I, AFM-II, AFM-III and FM. Here, the band structures for AFM-1, AFM-II and AFM-III are shown in Fig. S1 (a), (b), (c). The AFM-I is spin-polarized metal with Dirac point at $3\pi/5a$, similar to the FM configuration of the H-ZGNR-H. And the spin density distribution is also similar with the FM state of the H-14-H. The AFM-II is a spin-polarized metal without Dirac point. The AFM-III is nearly a spin-unpolarized metal with spin polarized states lying 4.06 eV above the Fermi energy.

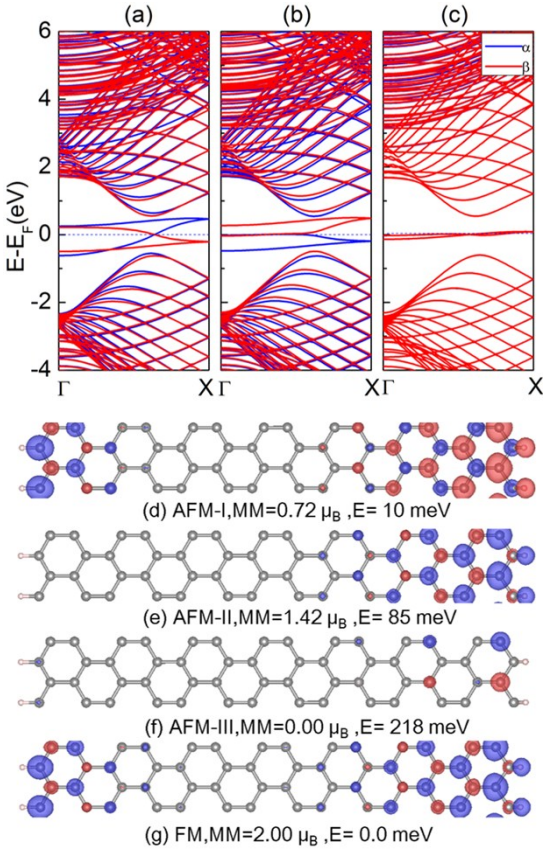

Fig. S1 The band structures and corresponding spin densities of the H-14-2H ZGNR with the different magnetic configurations (d) AFM-I, (e) AFM-II, (f) AFM-III and (g) FM calculated by PBE. The isovalue is set to 0.06 e/Å^3. The ferromagnetic configuration is

the lowest energy state. So its energy is set to be zero, and taken as energy reference for other magnetic configurations.

2. Normal ZGNRs show characters of strong localized electrons at the edge of the ribbons. For the H-M-LD-N-2H, there is a similar feature. In order to show the localized states of the H-M-LD-N-2H, we plot the distributions of the charge densities in the Fig. S2. Due to the existence of the localized electrons, these systems should be calculated by HSE06 for more accurate results.

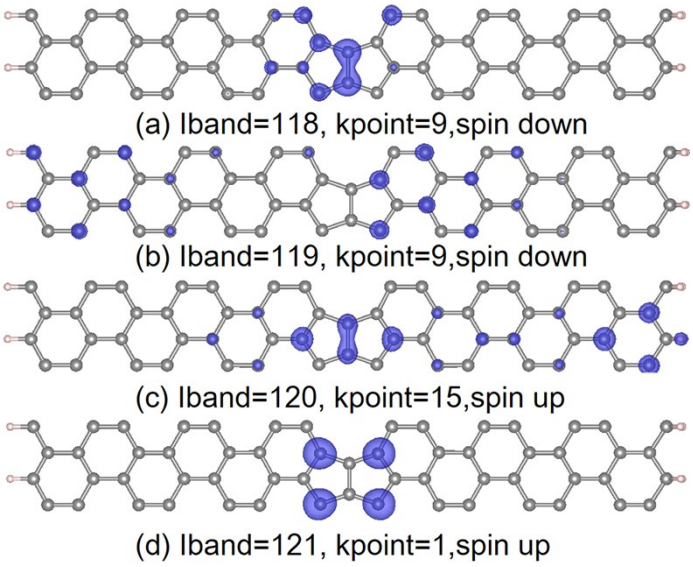

Fig. S2 The distributions of the charge densities of the certain bands at the special kpoints of the Brillouin zone. Spin-down electrons of (a) Iband=118, kpoints=9 (k=3π/5a), (b) Iband=119, kpoints=9 (k=3π/5a) 9. Spin-up electrons of (c) Iband=120, kpoints=15 (k=π/a, X point) and (d) Iband=121, kpoints=1 (k=0, Γ point).

3. In the article, we have discussed the charge densities of the VBM and CBM of the H-ZGNR-2H. But the electronic properties, for example, the VBM and CBM of the H-LD-H ZGNRs are not presented. With the reference of (a) band structure of a perfect H-15-H, we provide the (b) band structure and (c) PDOS of the H-6-LD-6-H. The charge densities of VBM are

shown in (d) and (f), and charge densities of CBM of the H-6-LD-6-H are shown (e) and (g), respectively.

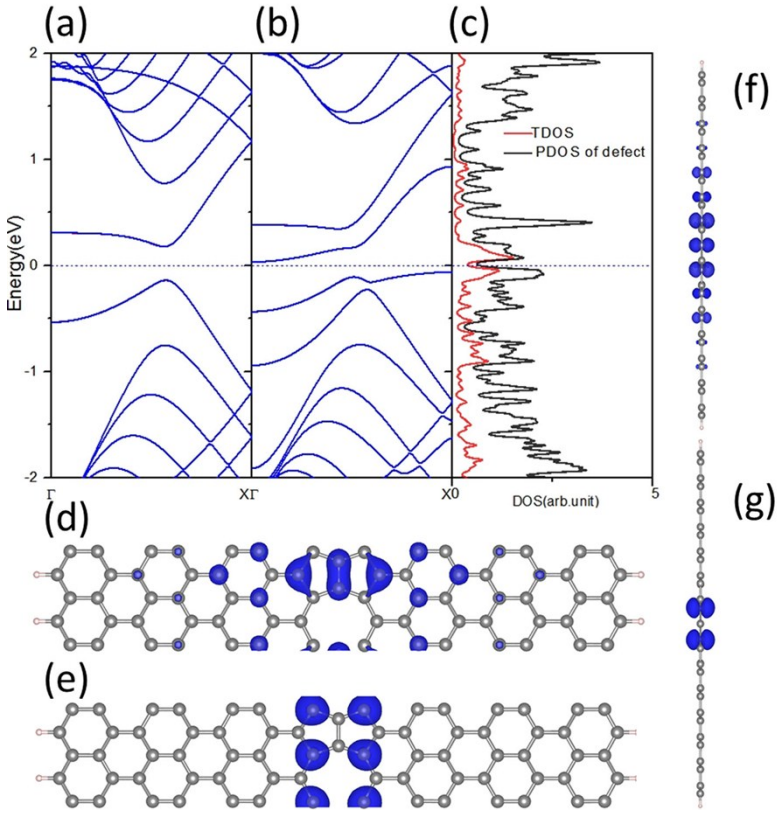

Fig. S3 The band structures of the (a) perfect H-15-H (ZGNR), (b) H-6-LD-6-H ZGNR, and (c) PDOS of the H-6-LD-6-H. The black and red lines are for the total DOS and PDOS of the line-defect atoms, respectively. The Fermi level is set to be 0. The top and side views of the charge density distributions of the VBM are shown in (d) and (f). And the top and side views of charge density distribution of CBM are shown in (e) and (g), respectively. The isovalue is set to 0.5 e/Å^3.

4. We have calculated the band structure of the H-4-LD-5-2H, which is found to be half-metallic with the FM ground state. The α-spin electron is metallic, while the β-spin electron is semiconducting. We further investigate the H-4-LD-7-2H and H-4-LD-9-2H using PBE, and the band structures are shown in Figs. S4 (a) (b), respectively. The H-4-LD-7-2H and H-

4-LD-9-2H are half-metals. This means that for certain configurations (M > 3 and N > 3), the H-N-LD-M-2H ZGNRs are half-metal no matter the ZGNRs are "symmetrical" ones or not.

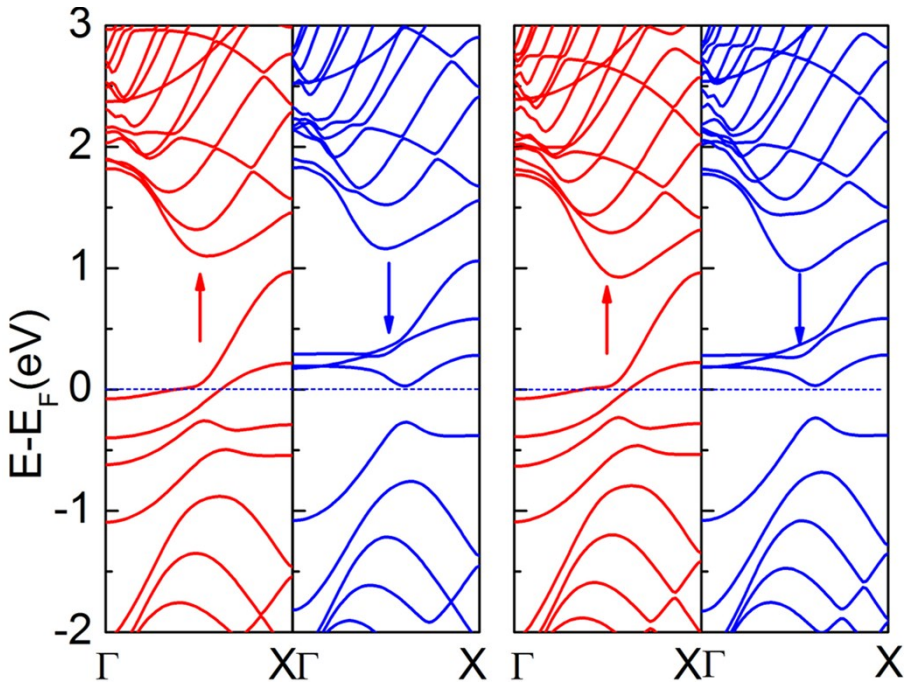

Fig. S4 The band structures of (a) H-4-LD-7-2H and (b) H-4-LD-9-2H calculated by PBE. The red and blue lines are for the α-spin and β-spin electrons, respectively. The Fermi level is set to zero.

5. In this article, we mainly discuss the electronic and magnetic properties of the H-M-LD-N-2H, the electronic and magnetic properties of the 2 line-defects embedded in H-ZGNR-2H are not presented. So we also test two groups of the 2 line-defects embedded in H-ZGNR-2H. Taking H-2-LD-6-LD-2-2H for example, the spin densities, band structure and DOS are shown in Figs. S5 (a) (b) (c), respectively. The calculated band structure is consistent with the H-ZGNR-H embedded with 2 line-defects, which shows the spin-polarized metallic feature with Dirac point, similar with the H-2-LD-6-LD-2-H. That's easy to be understood: the line-defect with high concentration effectively destroys the conjugative structure of the H-

2-LD-6-LD-2-H ZGNR. As the precursor, H-2-LD-6-LD-2-H ZGNR is metal with Dirac point. Two or more line-defects will not only destroy the planner structure of the ribbon, but also decrease the thermal stability. So we don't systematically investigate the properties. The concentration of the line-defects could also be utilized to tune the properties of the H-ZGNR-2H.

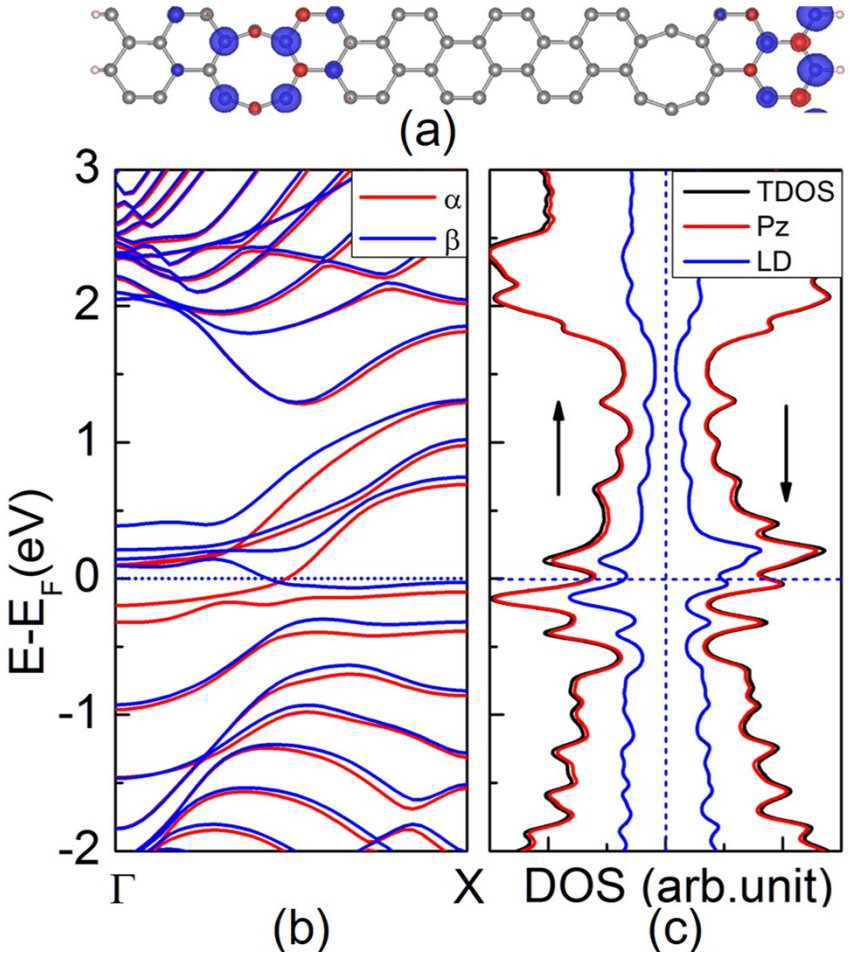

Fig. S5 (a) The spin densities, (b) band structure and (c) PDOS of the 2H-2-LD-6-LD-2-H. The isovalue is set to 0.06 e/ Å^3. For the PDOS, the black, red and blue lines are for the total DOS, PDOS of the p_z, and PDOS of the line-defect atoms, respectively.

6. We also calculate the band structure of H-M-LD-N-2H ZGNRs with M+N=8, and the corresponding band structures are shown in Fig. S6. For the smaller width, the position of the line-defect could also modulate the electronic properties of narrower H-M-LD-N-2H.

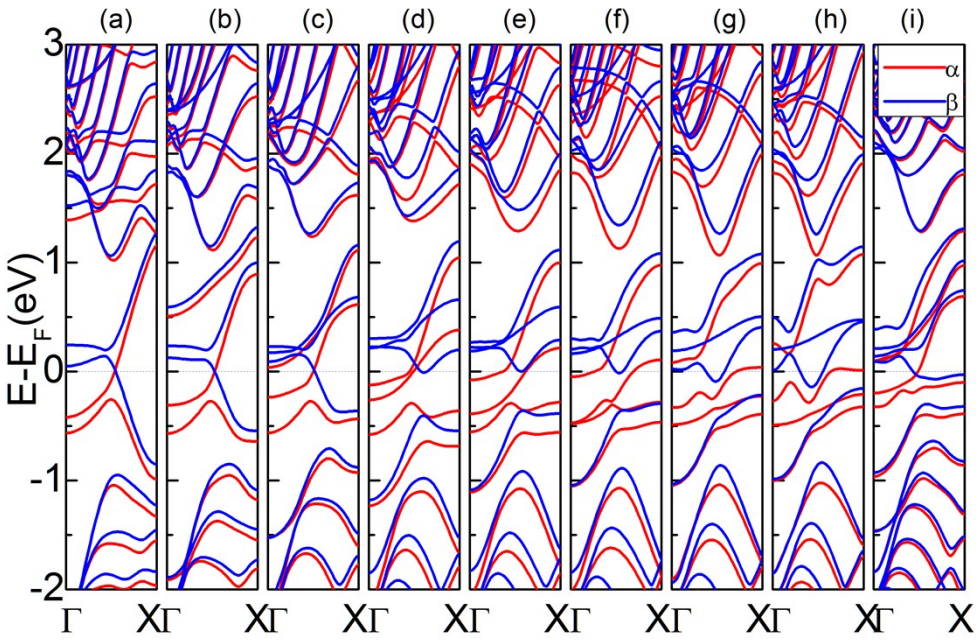

Fig. S6 The band structures of (a) H-8-LD-0-2H, (b) H-7-LD-1-2H, (c) H-6-LD-2-2H, (d) H-5-LD-3-2H, (e) H-4-LD-4-2H, (f) H-3-LD-5-2H, (g) H-2-LD-6-2H, (h) H-1-LD-7-2H, (i) H-0-LD-8-2H, calculated by PBE. The fermi level is set to 0 eV.

7. We also optimize structure of F-6-LD-6-2F, and the geometry is shown in Fig. S7. From the optimized structure, we can see that the F atoms distort edge obviously.

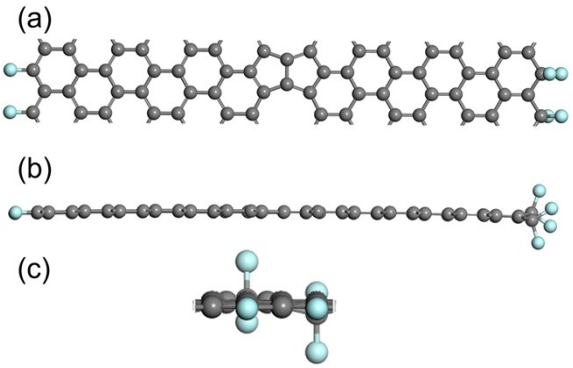

Fig. S7 (a) The top view, (b) and (c) side view of optimized structure F-6-LD-6-2F ZGNR.

8. We also calculate the spin density, band structure and DOS of the F-6-LD-6-2F ZGNR, with the results are shown in Fig. S8. The spin density of the edge functioned with two F atoms is suppressed for the obvious distortion. And the F-6-LD-6-2F ZGNR presents normal spin-polarized metallicity.

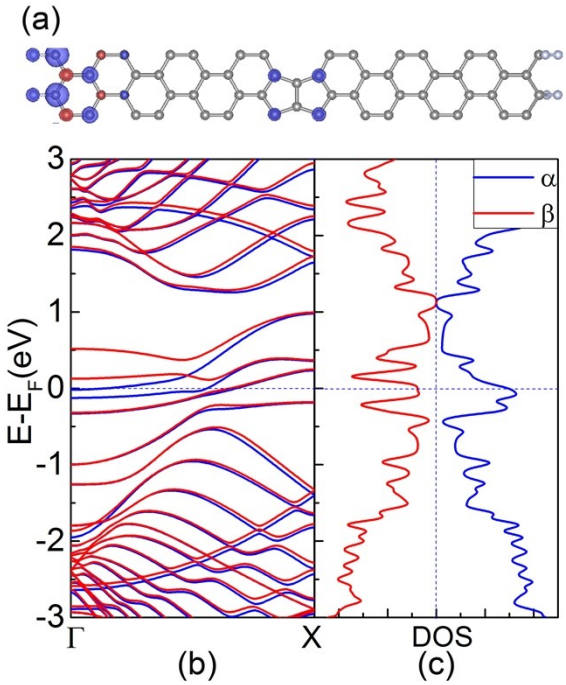

Fig. S8 The spin density of the F-6-LD-6-2F ZGNRs (a) ferromagnetic state. (b) and (c) present the band structure and TDOS of the F-6-LD-6-2F ZGNRs with PBE, respectively. The isovalues is set 0.06 e/ $Å^3$.

9. In order to confirm whether LDA calculations consistent results with the PBE's. We also recalculate H-14-2H and H-6-LD-6-2H ZGNRs with LDA. And the difference between the FM and AFM states is 8 meV (for H-14-2H). The band structure and density of the states with the FM ground states of H-14-2H, are shown in Fig. S9. The ground state is still FM sates with gap of 0.12 eV, comparing with the PBE functional (0.23 eV). The LDA often underestimates the band gaps for the localized electron approximation.

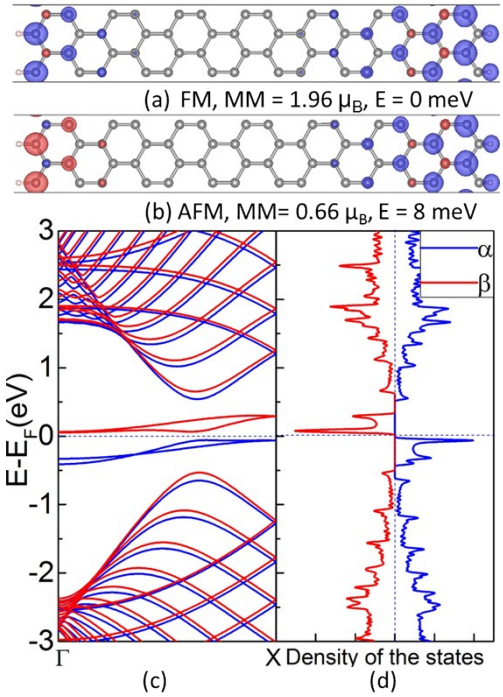

Fig. S9 The spin density of the H-14-2H ZGNRs (a) ferromagnetic state, (b) antiferromagnetic state. (c) and (d) present the band structure and TDOS of the H-14-2H ZGNRs with LDA. The isovalues is set 0.06 e/ $Å^3$. The energy of ferromagnetic state is set as reference.

10. The spin density of FM and AFM states of H-6-LD-6 ZGNR are also calculated with LDA approximation, which show the similar spin distribution with the PBE functional. The H-6-LD-6 ZGNR still present half-metallicity calculated by LDA.

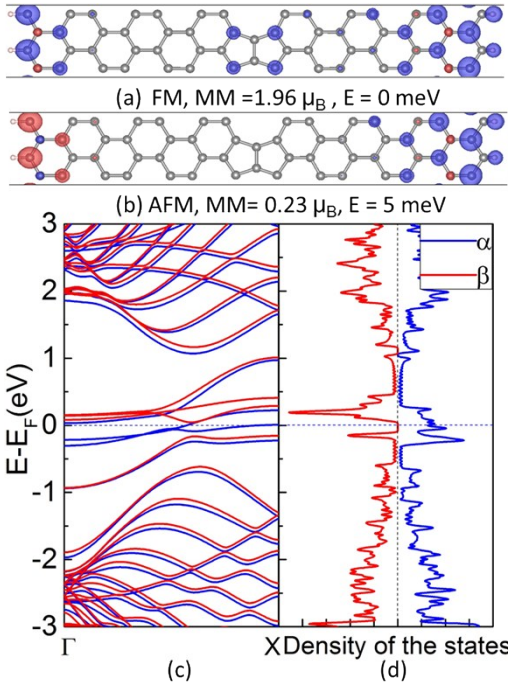

Fig. S10 The spin density of the H-6-LD-6-2H ZGNRs (a) ferromagnetic state, (b) antiferromagnetic state. (c) and (d) present the band structure and TDOS of the H-6-LD-6-2H ZGNRs with LDA. The isovalues is set 0.06 e/ $Å^3$.